

Multi-State Formulation of the Frozen-Density Embedding Quasi-Diabatization Approach

Patrick Eschenbach^{||}, Denis G. Artiukhin^{†1}, and Johannes Neugebauer^{||2}

^{||} Theoretische Organische Chemie, Organisch-Chemisches Institut and Center for
Multiscale Theory and Simulation, Westfälische Wilhelms-Universität Münster,
Corrensstraße 40, 48149 Münster, Germany

[†] Department of Chemistry, Aarhus Universitet, DK-8000 Aarhus, Denmark

Date: November 7, 2021

¹Email: artiukhin@chem.au.dk

²Email: j.neugebauer@uni-muenster.de

Abstract

We present a multi-state implementation of the recently developed FDE-diab methodology [*J. Chem. Phys.*, 148 (2018), 214104] in the SERENITY program. The new framework extends the original approach such that any number of charge-localized quasi-diabatic states can be coupled, giving an access to calculations of ground and excited state spin-density distributions as well as to excitation energies. We show that it is possible to obtain results similar to those from correlated wave function approaches such as the complete active space self-consistent field method at much lower computational effort. Additionally, we present a series of approximate computational schemes, which further decrease the overall computational cost and systematically converge to the full FDE-diab solution. The proposed methodology enables computational studies on spin-density distributions and related properties for large molecular systems of biochemical interest.

1 Introduction

The spin density is commonly defined as the difference of α and β electron densities and, thus, represents the excess of α electrons in a radical system. The accurate determination of the spin density is of high interest for both theory and experiment. Thus, in spin density functional theory (DFT), which is frequently used for open-shell molecular systems, both the electron and spin density are required for obtaining the exact ground-state energy [1]. Negative areas of the spin density are also an important ingredient in calculations of total squared spin operator expectation values $\langle S^2 \rangle$ (within the exchange local spin density approximation, see Ref. [2]), which can subsequently be used for the determination of magnetic exchange coupling constants [3, 4]. The latter play a major role in predicting magnetic interactions between, e.g., building blocks of organic radical crystals [5, 6]. Experimentally, spin-density maps can directly be measured with polarized neutron diffraction [7–9]. An indirect access to spin densities can be obtained with electron paramagnetic resonance (EPR) spectroscopy via the isotropic part of EPR hyperfine coupling constants, which depends on the spin-density contributions at atomic nuclei [10]. Specialized methods such as the solid-state photochemically induced dynamic nuclear polarization nuclear magnetic resonance and electron nuclear double resonance spectroscopy are also widely used for the determination of spin-density maps (for applications to cofactors from photosynthetic reaction centers, see Refs. [11–19]).

Although many experimental techniques can be used for the accurate determination of spin densities, theoretical computations of these molecular properties are challenging for most electronic structure methods [20–22]. Highly correlated *ab initio* wave function approaches are often used to calculate accurate spin densities and related properties such as EPR hyperfine coupling constants [23–27]. Unfortunately, these methods are computationally very demanding and, thus, not feasible for large molecular systems. This limitation is often lifted by using Kohn–Sham density functional theory (KS-DFT) [1]. However, it

is well known that KS-DFT suffers from the self-interaction error [28–30], which often leads to overdelocalized spin-density distributions, especially in cases of non-covalently bonded molecular systems [31,32]. This issue can be mitigated employing hybrid exchange–correlation (XC) functionals, which incorporate exact Hartree–Fock (HF) exchange [22]. On the downside, however, increasingly large areas of negative spin density and increasing spin contamination are observed in this case [33–39]. Additionally, the use of hybrid XC functionals can lead to “broken-symmetry-like” solutions providing qualitatively wrong spin densities as was shown for iron-nitrosyl complexes in Ref. [22].

The overdelocalization problem of KS-DFT can pragmatically be avoided by using the Frozen-Density Embedding (FDE) formalism [40–43]. FDE employs an additional non-additive kinetic energy potential (NAKP) and is, therefore, an approximation to KS-DFT. When the exact NAKP is used within FDE, both FDE and KS-DFT provide the same charge- and spin-density distributions (given that the same XC functional and basis set are applied) [37,38,44]. In practice, however, approximate NAKPs are commonly employed. These approximate potentials are often repulsive in the intermolecular regime and could, therefore, prevent charge- and spin-density delocalization over subsystem boundaries [32]. Although the use of a supermolecular basis set increases the degree of delocalization, this effect is rather modest. In fact, it can even be argued that the use of FDE leads to the opposite problem of overly localized spin-density distributions [45].

Recently, the FDE-diab approach for accurate calculations of spin densities was proposed [45]. This methodology is based on the previously known FDE-ET [37,46–48], and employs ideas of constructing charge- and spin-localized states with FDE and coupling them in a configuration interaction (CI)-like manner. It was demonstrated that this procedure avoids the consequences of KS-DFT spin overdelocalization error and does not lead to overly localized spin distributions characteristic for FDE. FDE-diab spin densities were compared against accurate *ab initio* computations [45] and experimental

measurements [49, 50]. A good qualitative agreement was found in all cases proving that the proposed methodology is accurate and effective. However, the program implementation available to date is limited to only two quasi-diabatic states. This severely restricts the applicability of FDE-diab and prevents one from calculations of supramolecular systems, where spin may naturally be delocalized over multiple fragments. In this work, we aim at filling this gap and present a multi-state extension of FDE-diab. To that end, we describe the underlying theory of this new approach, thoroughly test it on a number of model molecular systems, and demonstrate approximate schemes which decrease the overall computational cost and extend the applicability of the method towards larger molecular systems. We show that the proposed methodology is not limited by calculations of ground electronic state spin-density distributions but can also be used to obtain electronic couplings, excitation energies, as well as spin distributions in excited electronic states.

This work is structured as follows. In Sec. 2, the underlying theory of multi-state FDE-diab and derived approximate approaches is briefly summarized. Computational details are given in Sec. 3 and followed by results presented in Sec. 4. Finally, conclusions are drawn in Sec. 5.

2 Theory

In the following, the theory behind the FDE-diab approach [37, 45–48] is briefly introduced with a focus on the use of multiple quasi-diabatic states. Special attention is given to various approximations which can be invoked within the FDE-diab framework. For a more detailed explanation of underlying theoretical concepts, the reader is referred to the original works and Sec. S1 of the Supporting Information (SI).

2.1 FDE-diab for Multiple Electronic States

Within the multi-state formulation of FDE-diab, each adiabatic electronic wave function Ψ_m is represented as a linear combination of n quasi-diabatic states Φ_i ,

$$\Psi_m = B_{1m}\Phi_1 + B_{2m}\Phi_2 + \cdots + B_{nm}\Phi_n, \quad (1)$$

where B_{im} are linear combination coefficients. The quasi-diabatic states Φ_i are constructed as direct products (similar to those described in Refs. [51, 52]) of subsystem Slater determinants $|A\rangle$, $|B\rangle$, etc.,

$$\Phi_i = |A\rangle \otimes |B\rangle \otimes \cdots = |AB\dots\rangle, \quad (2)$$

which are obtained from prior FDE [40] calculations of the corresponding subsystems A , B , etc. In these FDE calculations, an electronic charge can be localized at a particular molecular fragment giving rise to different charge-localized states Φ_i . Additionally, subsystems in their electronically excited states can be considered [47]. To obtain molecular orbitals (MOs) comprising the mentioned above Slater determinants, the so-called Kohn–Sham equations with constrained electron density (KSCED) [40, 43, 53],

$$\left[-\frac{\nabla_i^2}{2} + v_{\text{KS}}^{I,\sigma}[\rho_I^\sigma](\vec{r}) + v_{\text{emb}}^{I,\sigma}[\rho_I^\sigma; \rho^{\text{tot},\sigma}](\vec{r}) \right] \phi_i^{I,\sigma}(\vec{r}) = \epsilon_i^{I,\sigma} \phi_i^{I,\sigma}(\vec{r}), \quad (3)$$

need to be solved. Here, $-\frac{\nabla_i^2}{2}$ is the one-electron kinetic energy operator, $v_{\text{KS}}^{I,\sigma}[\rho_I^\sigma](\vec{r})$ is the Kohn–Sham (KS) potential, and $v_{\text{emb}}^{I,\sigma}[\rho_I^\sigma; \rho^{\text{tot},\sigma}](\vec{r})$ is the embedding potential. $\phi_i^{I,\sigma}(\vec{r})$ and $\epsilon_i^{I,\sigma}$ are the KS-like MOs and orbital energies, respectively. I is the subsystem index, and $\sigma = \alpha$ or β is a spin label.

With the quasi-diabatic states Φ_i constructed, the linear combination coefficients B_{im} from Eq. (1) have to be found to calculate the adiabatic wave functions Ψ_m . To that end, a generalized eigenvalue problem in the basis of the quasi-diabatic states Φ_i is solved,

$$\mathbf{HB} = \mathbf{SBE}, \quad (4)$$

where \mathbf{H} and \mathbf{S} are the $n \times n$ Hamilton and overlap matrices, respectively. The matrix \mathbf{B} contains the linear combination coefficients B_{im} , and \mathbf{E} is a diagonal matrix of electronic energies E_m . The elements S_{ij} of the overlap matrix \mathbf{S} are defined as [54, 55],

$$S_{ij} = \langle \Phi_i | \Phi_j \rangle = \det \left(\mathbf{S}^{(ij),\alpha} \right) \det \left(\mathbf{S}^{(ij),\beta} \right). \quad (5)$$

Here, $\mathbf{S}^{(ij),\sigma}$ are the MO overlap matrices with elements $\left(\mathbf{S}^{(ij),\sigma} \right)_{kl}$ given by

$$\left(\mathbf{S}^{(ij),\sigma} \right)_{kl} = \left\langle \phi_k^{(i),\sigma} \middle| \phi_l^{(j),\sigma} \right\rangle. \quad (6)$$

The orbitals $\phi_k^{(i),\sigma}$ and $\phi_l^{(j),\sigma}$ belong to the quasi-diabatic states Φ_i and Φ_j , respectively. Because a monomer basis set is used for construction of quasi-diabatic states in FDE-diab (for examples, see Refs. [37, 45]), MOs of different subsystems are not orthogonal to each other. Therefore, the off-diagonal matrix elements from Eq. (6) differ from zero. The Hamilton matrix elements H_{ij} from Eq. (4) are approximated by calculating an KS energy functional of the transition electron density $\rho^{(ij)}(\vec{r})$ and scaling it by the overlap S_{ij} [37, 46–48],

$$H_{ij} = \left\langle \Phi_i \middle| \hat{H} \middle| \Phi_j \right\rangle \approx E \left[\rho^{(ij)}(\vec{r}) \right] S_{ij}. \quad (7)$$

The α - and β -components of the transition electron density $\rho^{(ij)}(\vec{r})$ are obtained by applying the corresponding electron density operators to quasi-diabatic wave functions Φ_i such that

$$\rho^{(ij),\sigma}(\vec{r}) = \frac{\langle \Phi_i | \hat{\rho}^\sigma | \Phi_j \rangle}{\langle \Phi_i | \Phi_j \rangle}, \quad (8)$$

where expressions for operators $\hat{\rho}^\sigma$ are given by

$$\hat{\rho}^\sigma = \sum_{l=1}^{N_{\text{el}}} \left[\frac{1}{2} \hat{\mathbf{1}}_l \pm \hat{s}_{z,l} \right] \delta(\vec{r}_l - \vec{r}). \quad (9)$$

Here, $\hat{\mathbf{1}}_l$ and $\hat{s}_{z,l}$ are the identity operator and the z -component of the spin operator \hat{s}_l , respectively, both acting on electron l . $\delta(\vec{r}_l - \vec{r})$ is the Dirac delta function and N_{el} is the number of electrons. The plus sign in square brackets of Eq. (9) corresponds to the $\hat{\rho}^\alpha$ operator, whereas the minus sign produces $\hat{\rho}^\beta$. The resulting density $\rho^{(ij),\sigma}(\vec{r})$ is expressed

in terms of non-orthogonal MOs $\{\phi_k^{(i),\sigma}\}$ and $\{\phi_l^{(j),\sigma}\}$ and elements of the transposed and inverse overlap matrix $\mathbf{S}^{(ij),\sigma}$ such that [37, 46–48]

$$\rho^{(ij),\sigma}(\vec{r}) = \sum_{k,l=1}^{N_{\text{el}}^{\sigma}} \phi_k^{(i),\sigma}(\vec{r}) \left(\mathbf{S}^{(ij),\sigma}\right)_{lk}^{-1} \phi_l^{(j),\sigma}(\vec{r}). \quad (10)$$

Here, the indices k and l refer to MOs used for construction of Slater determinants Φ_i and Φ_j , respectively. Note that these indices are interchanged for the overlap matrix $\mathbf{S}^{(ij),\sigma}$ denoting transposition. Alternatively, this expression can be given as,

$$\rho^{(ij),\sigma}(\vec{r}) = \sum_{I,J=1}^M \sum_{k \in I} \sum_{l \in J} \phi_k^{(i),\sigma}(\vec{r}) \left(\mathbf{S}^{(ij),\sigma}\right)_{lk}^{-1} \phi_l^{(j),\sigma}(\vec{r}), \quad (11)$$

where the first sum runs over all M subsystems used for the constructions of quasi-diabatic states, while the second and third sums run over MOs belonging to subsystems I and J , respectively.

After obtaining all necessary components for Eq. (4), the linear combination coefficients B_{im} and energies E_m of the adiabatic wave functions Ψ_m can be calculated. The obtained linear combination coefficients B_{im} can be used to construct n adiabatic wave functions Ψ_m . From these wave functions other molecular properties such as, for example, the spin-density distribution can be calculated [45, 49, 50]. To that end, expectation values of the α - and β -density operators need to be computed,

$$\rho_m^{\sigma}(\vec{r}) = \frac{\langle \Psi_m | \hat{\rho}^{\sigma} | \Psi_m \rangle}{\langle \Psi_m | \Psi_m \rangle} = \frac{\sum_{i,j}^n B_{im} B_{jm} \rho^{(ij),\sigma} S_{ij}}{\sum_{i,j}^n B_{im} B_{jm} S_{ij}}. \quad (12)$$

Here, Eqs. (1), (5), and (10) were applied. The resulting spin density $\rho_m^{\alpha-\beta}(\vec{r})$ of electronic state m is then calculated as a difference of its α - and β -components,

$$\rho_m^{\alpha-\beta}(\vec{r}) = \rho_m^{\alpha}(\vec{r}) - \rho_m^{\beta}(\vec{r}). \quad (13)$$

The spin-density calculated in this way was compared against accurate *ab initio* results [45] and experimental measurements [49, 50] showing a good qualitative agreement in both cases.

2.2 Approximate FDE-diab

As can be seen from Eq. (2), the quasi-diabatic states are constructed from Slater determinants of all subsystems' MOs. Thus, calculations of the inverse overlap matrix $(\mathbf{S}^{(ij),\sigma})^{-1}$ from Eq. (10) and Hamilton matrix elements H_{ij} from Eq. (7) are carried out in the orbital space of the total molecular system. The overall computational cost of FDE-diab, therefore, grows rapidly with the number of MOs and subsystems considered and becomes prohibitively large for large (bio-)molecular systems. In order to tackle this issue, different approximations can be invoked. One of such approaches was proposed in Ref. [46] and is motivated by large differences between inter- and intra-subsystem MO overlaps. To demonstrate this, we introduce subsystem MO overlap matrices $\mathbf{S}_{IJ}^{(ij),\sigma}$ as (for more detail on the block-structure of $\mathbf{S}^{(ij),\sigma}$, see Sec. S1 in the SI),

$$\left(\mathbf{S}_{IJ}^{(ij),\sigma}\right)_{kl} = \left\langle \phi_{k \in I}^{(i),\sigma} \left| \phi_{l \in J}^{(j),\sigma} \right. \right\rangle, \quad (14)$$

where MOs $\phi_{k \in I}^{(i),\sigma}$ belong to subsystem I and correspond to quasi-diabatic state Φ_i . Because the elements of intra-subsystem overlap matrices $\mathbf{S}_{II}^{(ij),\sigma}$ are typically much larger than those of inter-subsystem counterparts $\mathbf{S}_{IJ}^{(ij),\sigma}$, the latter can be set to zero giving rise to a modified form of Eq. (11),

$$\rho^{(ij),\sigma}(\vec{r}) \approx \sum_{I=1}^M \rho_I^{(ij),\sigma}(\vec{r}) = \sum_{I=1}^M \sum_{k \in I} \sum_{l \in I} \phi_k^{(i),\sigma}(\vec{r}) \left(\mathbf{S}_{II}^{(ij),\sigma}\right)_{lk}^{-1} \phi_l^{(j),\sigma}(\vec{r}). \quad (15)$$

The obtained transition density $\rho^{(ij),\sigma}(\vec{r})$ is equal to the sum of subsystem transition densities $\rho_I^{(ij),\sigma}(\vec{r})$, thus, leading to linear scaling (with the number of subsystems) of FDE-diab [46]. However, this approach is not capable of describing inter-subsystem spin-density delocalization and charge-transfer processes. This limitation can partially be lifted by introducing a subset of subsystems \mathcal{L} (undergoing charge-transfer or featuring spin delocalization) and explicitly considering the contributions from their MO overlaps. In other words, we set $\mathbf{S}_{IJ}^{(ij),\sigma}$ to zero if both requirements $I \neq J$ and $I, J \notin \mathcal{L}$ are satisfied. This approach was successfully applied in Ref. [46] for charge-transfer simulations occurring between two subsystems.

Alternatively, reduction in the overall computational cost can be achieved by decreasing the number of subsystems M , as seen in Eq. (11), used for the construction of quasi-diabatic states. In this case, the electron density of the total system can still be relaxed within FDE by means of freeze-and-thaw cycles [41], but only the MO coefficients of the chosen subsystems are used in the subsequent FDE-diab computation. This approximation was previously employed for calculations of spin-density distributions in photosynthetic cofactors embedded in large parts of the protein environment and showed good agreement with available experimental results [49, 50]. It should also be noted that additional minor computational savings can be obtained by considering a subset of the constructed quasi-diabatic states in the solution of the generalized eigenvalue problem from Eq. (4). The above-mentioned techniques can, in principle, be combined producing various approximate FDE-diab computational schemes. For these calculations, we adopt the FDE-diab(K, L, M) notation. Here, K stands for the number of quasi-diabatic electronic states considered while solving the generalized eigenvalue problem, L is the number of subsystems with non-zero inter-subsystem MO overlaps (from \mathcal{L}), and M is the number of subsystems used for the construction of quasi-diabatic states. Thus, if a molecular system $[ABCDE]^{\bullet+}$ is considered, one might solve a 2×2 eigenvalue problem coupling only electronic states $|A^{\bullet+}BCD\rangle$ and $|AB^{\bullet+}CD\rangle$ embedded in environment E , where non-zero inter-subsystem MO overlaps are employed for A , B , and C . This procedure can then be denoted as FDE-diab(2,3,4), while the reference non-approximate FDE-diab computation would correspond to FDE-diab(5,5,5). In the following, if not stated otherwise, non-approximate FDE-diab computations will be denoted simply as FDE-diab.

3 Computational Details

The structures of the deoxyribonucleic acid (DNA) base triplets guanine–thymine–guanine (GTG) and guanine–adenine–guanine (GAG), molecules from the HAB11 benchmark set,

and those presented in Sec. S2.2 in the SI were taken from Refs. [45, 56, 57], respectively, and used without further optimization. The benzene octamer molecular structure was created with the AVOGADRO program [58] and fully optimized using the TURBOMOLE v7.4.1 program package [59] with C_{2h} symmetry. In this calculation, the valence polarized triple- ζ Def2-TZVP basis set [60, 61] and the XC functional PBE0 [62, 63] were employed. Additionally, the resolution-of-the-identity (RI) approximation in conjunction with the auxiliary Coulomb fitting valence triple- ζ basis Def2-TZV/J [60, 61] was enabled. Dispersion interactions were taken into account using the D3BJ correction with Becke–Johnson damping [64, 65].

Calculations of spin-density distributions and electronic couplings were carried out with SERENITY [66] and ADF [67, 68] program packages. All SERENITY calculations were performed using the Def2-TZVP and auxiliary Coulomb fitting Def2-TZV/J basis sets under the RI approximation. In the case of ADF, the triple- ζ TZP [69] monomer basis set from the ADF basis set library was used. KS-DFT calculations of spin-density distributions were carried out with SERENITY using the generalized-gradient approximation (GGA) PBE [70], hybrid B3LYP (20% exact exchange) [71–74], range-separated hybrid CAM-B3LYP (19% exact exchange) [75], and double-hybrid B2PLYP (53% exact exchange) [76] functionals. In cases of FDE-diab/FDE-ET [37, 45–48] calculations, locally modified versions of the SERENITY [66] and ADF [67, 68] program packages were applied. In these computations, the XC functional PW91 [77, 78] with the conjoint [79] kinetic-energy functional PW91k [80] were adopted. Relaxation of subsystem densities was accounted for using freeze-and-thaw cycles [41]. Three such cycles were found sufficient to obtain accurate electron densities. Spin contamination of adiabatic multi-state FDE-diab wave functions was calculated with SERENITY employing the corresponding densities for computations of the $\langle S^2 \rangle$ value (for more details, see Ref. [2]).

To provide a quantitative measure for the spin-density delocalization, a Becke-type pop-

ulation analysis was carried out with the ADF and SERENITY programs following the procedure used in our previous works (e.g., see Ref. [39]). To that end, accurate atom-centered Becke grids [81–83] were generated. Grid points were assigned to particular nuclei forming overlapping atomic-basins. The spin-density values at grid points were integrated over atomic-basins yielding atomic spin-density populations. The reported molecular spin-density populations (in percent) were calculated by summing up the corresponding atomic contributions over subsystems.

Reference spin-density distributions of the [GTG]^{•+} and [GAG]^{•+} radical cations were computed with CASSCF [84–86]. These calculations were performed in OPENMOLCAS [87, 88] using Dunning’s correlation-consistent cc-pVDZ basis set of double- ζ quality [89, 90]. Restricted HF orbitals of neutral molecules around the HOMO–LUMO gaps provided an initial guess for the CASSCF calculations of the corresponding radical cations. All multiconfiguration calculations were carried out in a state-specific manner. The notation CAS(l, k)-SCF was adopted in this work, where l and k stand for the numbers of active space electrons and orbitals, respectively. Converged spin-density distributions were obtained with CAS(15,16)-SCF.

4 Results

In the following, we first present an in-depth comparison of various properties calculated with the two-state FDE-diab implementation in the SERENITY program and with that from ADF in Sec. 4.1. Second, the performance of the new multi-state FDE-diab approach for spin densities of non-covalently bonded DNA base triplet radical cation complexes is demonstrated and compared against KS-DFT and reference CASSCF in Sec. 4.2. Finally, in Sec. 4.3 we present three approximate multi-state FDE-diab schemes systematically converging to the full FDE-diab results in the limit of all couplings, subsystems, and

overlaps being considered explicitly.

4.1 Two-State FDE-diab: Comparison of ADF and Serenity

To validate the two-state FDE-diab implementation in the SERENITY program, we calculated a variety of different properties and compared them with those obtained with ADF. The calculated quantities included: i) electronic couplings for 11 dimeric molecular radical cation complexes at different intermolecular displacements (benchmarked with ADF in Ref. [48]) from the HAB11 set [57] and ii) spin densities and atomic spin populations for dimeric molecular complexes presented in Ref. [45]. The complete set of calculated values is given in Sec. S2 in the SI, while here we only briefly discuss the overall two-state FDE-diab performance for electronic couplings and atomic spin populations. It should be noted that Slater-type basis functions (STOs) are used in the ADF program, whereas Gaussian-type basis functions (GTOs) are employed in SERENITY. Therefore, small differences between values calculated with ADF and SERENITY are expected.

Root-mean square deviations (RMSDs) of absolute values of electronic couplings calculated with SERENITY and ADF are shown in Fig. 1 a), while mean absolute percentage errors (MAPEs) are presented in Fig. 1 b). As can be seen from Fig. 1 a), electronic couplings calculated with both program packages are in a good agreement and show rather small deviations from each other (for values of electronic couplings, see Sec. S2.1 in the SI). Thus, the largest RMSD equal to about 11 meV is found for the intermolecular distance of 3.5 Å. For larger distances, the RMSD decreases and reaches about 3 meV at the separation of 5.0 Å. An opposite trend is observed for MAPE, which increases with the intermolecular distance. However, the largest deviations is equal to only about 5%.

Atomic spin populations calculated with SERENITY and ADF for complexes from Ref. [45] are also in a very good agreement as seen from Fig. 1 c). The largest RMSDs of about 0.05

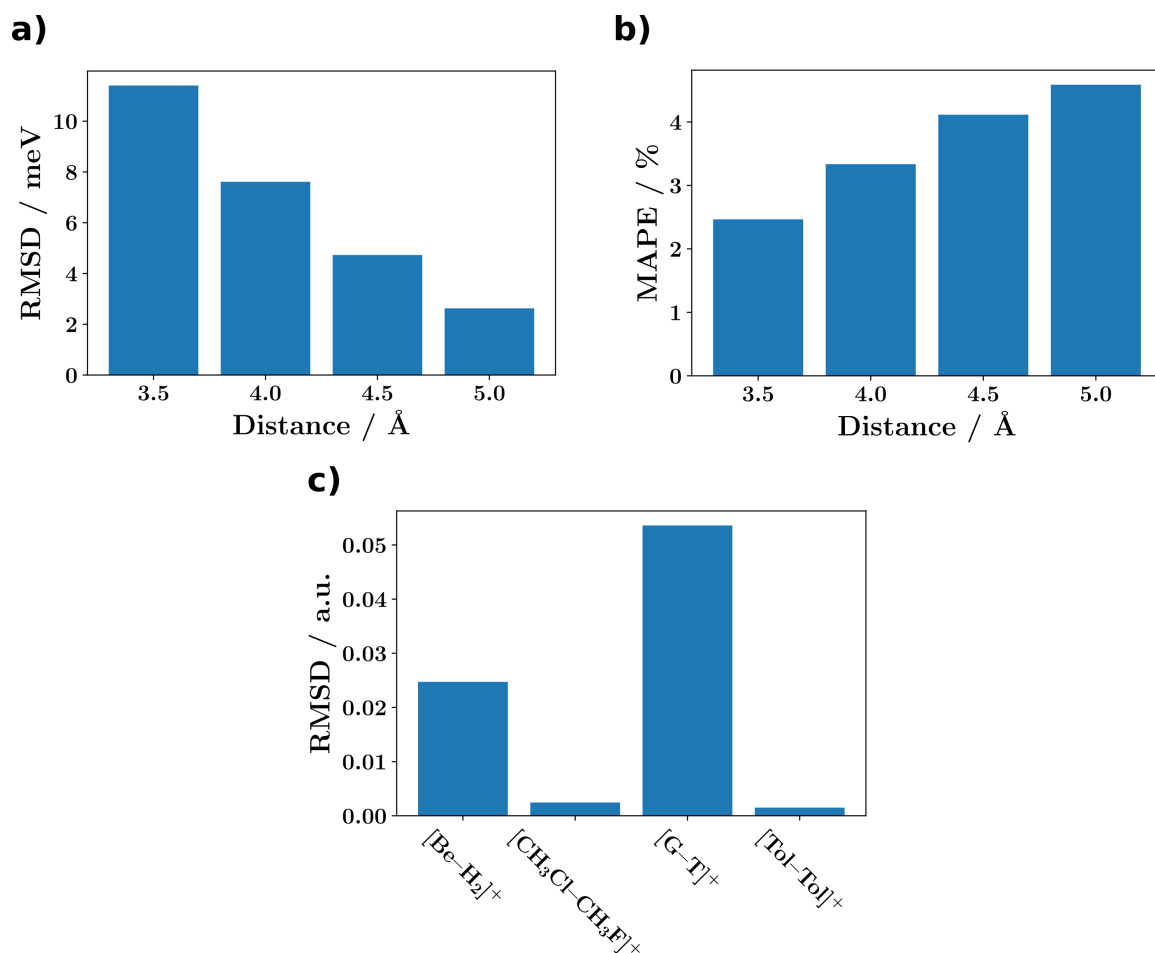


Figure 1: Comparison of absolute electronic couplings and atomic spin populations calculated with SERENITY and ADF. Results shown are a) RMSDs of absolute electronic couplings (in meV) for molecules from the HAB11 benchmark set at different intermolecular distances, b) corresponding MAPEs, and c) RMSDs of atomic spin populations (in a.u.) for four radical cation complexes from Ref. [45].

and 0.02 a.u. are obtained for $[G-T]^{\bullet+}$ and $[Be-H_2]^{\bullet+}$, respectively. For the other two complexes, deviations are very small and are below 0.002 a.u. For spin-density isoplots and molecular spin populations, see Fig. S2 in the SI. Errors in other quantities calculated with SERENITY are also in a good agreement with those from ADF (see Sec. S2 in the SI). Therefore, we conclude the FDE-diab implementation in SERENITY established in this work produces very similar results to the reference implementation in ADF [45, 46] with

rather small differences caused by different-type basis sets used.

4.2 Multi-State FDE-diab for DNA Base Triplets

Charge- and hole-transfer processes in π -stacked DNA nucleobases received considerable attention in the literature. In the case of small radical cation complexes containing two and three nucleobases, many molecular properties such as electronic couplings, charge distributions, and excitation energies are well-studied and available (e.g., see Refs. [56,91]). This makes them very good testing examples for the multi-state FDE-diab framework. In the following, we present FDE-diab computations for the radical cation complexes of the DNA base triplets $[G_1TG_2]^{\bullet+}$ and $[G_1AG_2]^{\bullet+}$. To distinguish between the two guanine fragments, we label them G_1 and G_2 in both complexes. We compare FDE-diab results against those obtained with KS-DFT and CASSCF. The CASSCF method has been frequently applied for accurate calculations of spin densities in the past (for examples, see Refs. [22,39]) and serves as the reference in this work. In FDE-diab calculations, three quasi-diabatic states of the form $\Phi_1 = |G_1^{\bullet+}BG_2\rangle$, $\Phi_2 = |G_1B^{\bullet+}G_2\rangle$ and $\Phi_3 = |G_1BG_2^{\bullet+}\rangle$, where B is adenine or thymine, were constructed. Solving the eigenvalue problem in the basis of these quasi-diabatic states, three adiabatic wave functions were obtained: The ground state Ψ_0 and first two excited states Ψ_1 and Ψ_2 . These wave functions were then used to obtain various molecular properties.

The $[G_1AG_2]^{\bullet+}$ and $[G_1TG_2]^{\bullet+}$ ground state spin-density distributions calculated with KS-DFT, FDE-diab, and CAS(15,16)-SCF are shown in Figs. 2 and 3, respectively, whereas molecular spin-density populations and $\langle S^2 \rangle$ expectation values are given in Tab. S15 in the SI. As one can see, the reference CAS(15,16)-SCF spin densities of $[G_1AG_2]^{\bullet+}$ and $[G_1TG_2]^{\bullet+}$ are almost fully localized at the G_1 molecules. In the both complexes, A and T carry very small spin-density contributions of about 1–2%, while no spin distribution is found at G_2 . The spin density calculated with KS-DFT is strongly dependent on the XC

functional used. Similar results were previously reported in several works (for examples, see Refs. [32, 45]). The double hybrid B2PLYP functional shows the best agreement with the CASSCF reference and produces about 93% and 95% of spin being localized at G_1 in $[G_1AG_2]^{\bullet+}$ and $[G_1TG_2]^{\bullet+}$, respectively. However, in this case the corresponding $\langle S^2 \rangle$ expectation values are much larger than the exact value of 0.75 a.u. and point out at a high degree of spin contamination. The latter also results in overestimated areas of the negative spin density (compared to CASSCF) as seen from Figs. 2 and 3. This is expected as increasing amounts of the exact exchange often lead to larger spin contamination, which is directly related to the negative spin density [30, 33, 34, 36, 37, 39]. The use of CAM-B3LYP results in somewhat smaller spin contamination values, but strongly overestimates (by about 16–20%) the spin contributions at A in $[G_1AG_2]^{\bullet+}$ and G_2 in $[G_1TG_2]^{\bullet+}$. The most strongly delocalized spin distributions are calculated with the B3LYP functional. In the case of PBE, a very good agreement with the reference is found for the $[G_1AG_2]^{\bullet+}$ complex. The corresponding $\langle S^2 \rangle$ value is equal to about 0.85 a.u. and only slightly differs from the exact value of 0.75 a.u. However, the calculation of $[G_1TG_2]^{\bullet+}$ employing the PBE functional does not converge. As seen from Figs. 2 and 3, the FDE-diab spin-densities are largely localized at G_1 and, therefore, are in a good agreement with CAS(15,16)-SCF. Moreover, in the case of $[G_1TG_2]^{\bullet+}$ an excellent quantitative agreement (with deviations below 0.3%) is obtained for molecular spin populations (see Tab. S15). The $[G_1AG_2]^{\bullet+}$ molecular spin populations calculated with FDE-diab deviate from those computed with CAS(15,16)-SCF by about 3–9% with the largest error obtained for G_1 . For the both molecular complexes, the $\langle S^2 \rangle$ values calculated with FDE-diab are equal to about 0.84 a.u. and are, therefore, very close to the exact expectation value of 0.75 a.u. Summarizing the obtained results, we conclude that the new multi-state FDE-diab methodology is more robust than standard KS-DFT and, similarly to its two-state predecessor [45], leads to qualitatively correct spin distributions.

To show-case the capabilities of multi-state FDE-diab, we also present molecular spin

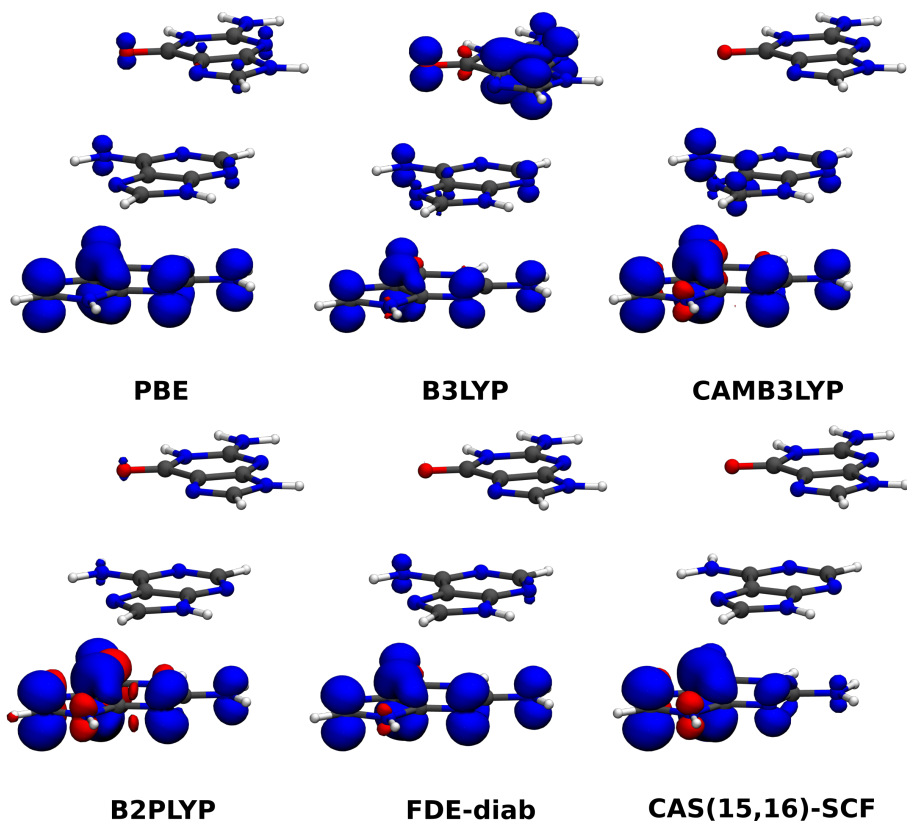


Figure 2: Spin-density distributions (isovalue ± 0.003 a.u.) of the $[G_1AG_2]^{\bullet+}$ radical cation complex. Blue and red colors represent positive and negative spin densities, respectively.

populations and total adiabatic energies obtained for the first two electronically excited states of $[G_1AG_2]^{\bullet+}$ and $[G_1TG_2]^{\bullet+}$ in Tab. 1. Here, CAS(11,12)-SCF computations reported in Ref. [56] were used as the reference. Additionally, spin-density distributions for the three lowest electronic states are given in Fig. S6 in the SI. As can be seen, in the first excited state of both complexes the FDE-diab spin density is mostly localized at G_2 , whereas T and A feature the largest spin distributions in the second excited state. These results agree well with CAS(11,12)-SCF computations. An excellent agreement between FDE-diab and CAS(11,12)-SCF molecular spin populations is obtained in the case of $[G_1TG_2]^{\bullet+}$, where the calculated values deviate by up to 1.5% and 0.2% for the first and second excited states, respectively. A somewhat worse performance of FDE-diab (compared to CAS(11,12)-SCF) is observed for $[G_1AG_2]^{\bullet+}$, where deviations of up to about

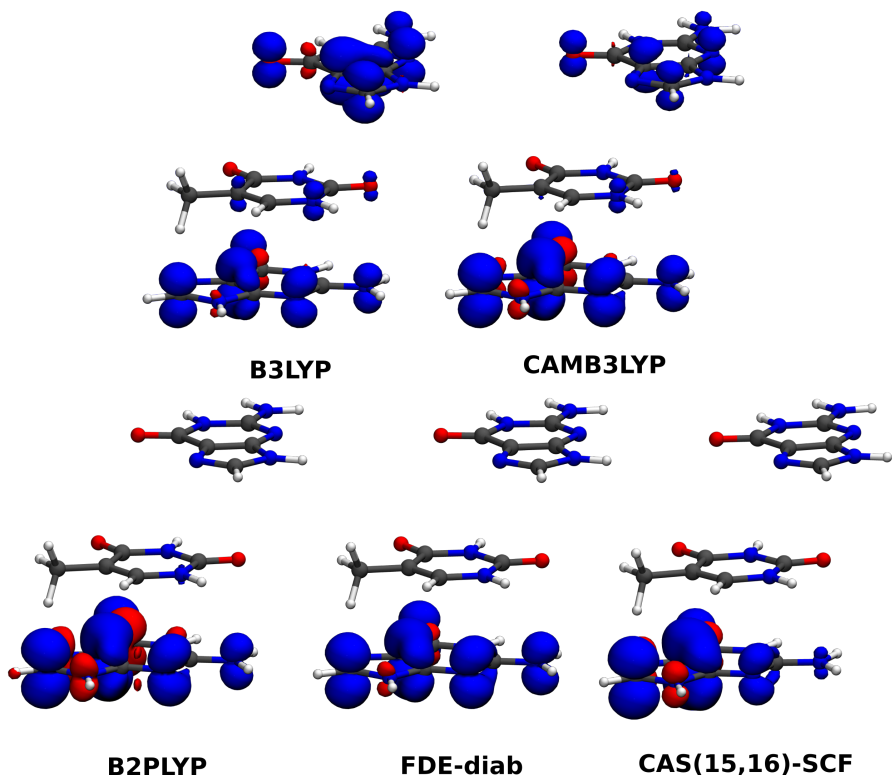


Figure 3: Spin-density distributions (isovalue ± 0.003 a.u.) of the $[G_1TG_2]^{\bullet+}$ radical cation complex. Blue and red colors represent positive and negative spin densities, respectively.

20% are found. In all FDE-diab computations presented, the $\langle S^2 \rangle$ value is equal to about 0.81–0.83 a.u. Therefore, the calculated spin-density distributions are only slightly spin contaminated. An opposite trend can be seen for energy values. Thus, the first two excited state energies of $[G_1AG_2]^{\bullet+}$ calculated with FDE-diab and CAS(11,12)-SCF deviate by less than 0.01 eV, whereas the second excited electronic state of $[G_1TG_2]^{\bullet+}$ shows a much larger difference of about 0.5 eV. It should be noted, however, that the observed deviations do not necessarily mean a bad performance of FDE-diab as a rather small active space and no perturbation energy correction were employed in the reference CASSCF calculations. On the opposite, qualitative agreements between FDE-diab and CASSCF molecular properties found for the three lowest electronic states is rather impressive. This may point out at the possibility to apply the FDE-diab computational approach as a less expensive but

still accurate enough alternative to very expensive CASSCF for spin-density and energy calculations of large molecular systems.

Table 1: FDE-diab and CAS(11,12)-SCF molecular spin populations $P(\text{nucleobase})$ and total adiabatic energies E (relative to the ground state energy E_0) of the $[\text{G}_1\text{AG}_2]^{\bullet+}$ and $[\text{G}_1\text{TG}_2]^{\bullet+}$ radical cation complexes in the first two excited electronic states (Ψ_1 and Ψ_2). CAS(11,12)-SCF results are taken from Ref. [56].

Electronic state	$P(\text{G}_1), \%$	$P(\text{B}), \%$	$P(\text{G}_2), \%$	E, eV
$[\text{G}_1\text{AG}_2]^{\bullet+}$				
$\Psi_1^{\text{FDE-diab}}$	8.4	17.0	74.5	0.12
$\Psi_2^{\text{FDE-diab}}$	3.0	75.4	21.6	0.35
Ψ_1^{CASSCF}	1.8	4.2	94.0	0.12
Ψ_2^{CASSCF}	3.7	90.7	5.7	0.34
$[\text{G}_1\text{TG}_2]^{\bullet+}$				
$\Psi_1^{\text{FDE-diab}}$	0.2	1.5	98.2	0.21
$\Psi_2^{\text{FDE-diab}}$	1.6	97.2	1.1	0.76
Ψ_1^{CASSCF}	0.6	0.0	99.4	0.18
Ψ_2^{CASSCF}	1.6	97.4	1.0	1.24

Finally, we demonstrate pair-wise electronic couplings calculated with the SERENITY program for $[\text{G}_1\text{AG}_2]^{\bullet+}$ and $[\text{G}_1\text{TG}_2]^{\bullet+}$ and compare them against those calculated with the generalized Mulliken–Hush method employing CAS(11,12)-SCF as reported in Ref. [56]. It has to be noted here that the FDE-ET module within the multi-state FDE-diab framework in the SERENITY program is similar to the original two-state FDE-ET [37,46–48] and has no multi-state capabilities. To this end, pairs of the generated quasi-diabatic states Φ_i and Φ_j (described above) were used as the basis for the generalized eigenvalue problem from Eq. (4). Using the notation system FDE-diab(K, L, M) introduced in Sec. 2.2, this approach can

be denoted as FDE-diab(2,3,3). The resulting electronic couplings V_{ij} are shown in Tab. 2. As one can see, the calculated absolute deviations for the $[\text{G}_1\text{TG}_2]^{\bullet+}$ complex are small and vary from about 0.001 to 0.02 eV. Somewhat larger differences of 0.01–0.05 eV are found for $[\text{G}_1\text{AG}_2]^{\bullet+}$. As was already stated above, CAS(11,12)-SCF does not employ a large enough active space of orbitals nor an energy perturbation correction. Therefore, decisive conclusions on the quality of the presented couplings cannot be made on the basis of available results. However, at this point we merely aim at demonstrating capabilities of the new extended framework. For more thorough benchmarks of electronic couplings, we refer the interested reader to the original works on the FDE-ET approach [37, 46–48].

Table 2: Absolute values of electronic couplings $|V_{ij}|$ for the $[\text{G}_1\text{AG}_2]^{\bullet+}$ and $[\text{G}_1\text{TG}_2]^{\bullet+}$ radical cation complexes. Results are presented for the FDE-diab methodology used in this work and the generalized Mulliken–Hush method employing CAS(11,12)-SCF from Ref. [56]. All values are given in eV.

	FDE-diab	CAS(11,12)-SCF	Difference
$[\text{G}_1\text{AG}_2]^{\bullet+}$			
$ V_{12} $	0.063	0.049	−0.014
$ V_{23} $	0.100	0.052	−0.048
$ V_{13} $	0.003	0.013	0.010
$[\text{G}_1\text{TG}_2]^{\bullet+}$			
$ V_{12} $	0.090	0.078	−0.012
$ V_{23} $	0.058	0.082	0.024
$ V_{13} $	0.000	0.001	0.001

4.3 Approximate Multi-State FDE-diab

Before demonstrating the efficiency and characteristics of approximate FDE-diab protocols, we first introduce our test example of a π -stacked benzene octamer complex (see Fig. 4). For this system, we construct a basis of eight quasi-diabatic states of the form $\Phi_1 = |B_1^{\bullet+} B_2 \cdots B_8\rangle$, $\Phi_2 = |B_1 B_2^{\bullet+} \cdots B_8\rangle$, \dots , $\Phi_8 = |B_1 B_2 \cdots B_8^{\bullet+}\rangle$, where B stands for benzene. According to the non-approximate FDE-diab approach, i.e., in this case FDE-diab(8,8,8) (for the notation, see Sec. 2.2), the largest spin-density contributions of about 29–32% each are localized on the benzene molecules with indices 4 and 5. Smaller molecular spin populations equal to about 14–18% are obtained for benzene molecules 3 and 6, whereas benzene molecules 2 and 7 carry only 3–4% of the unpaired spin. Negligible amounts of the spin density (below 1%) are found at molecules 1 and 8.

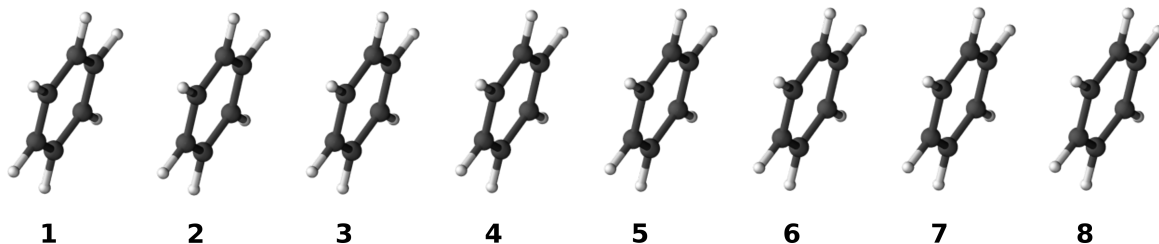


Figure 4: Graphical representation of the π -stacked benzene octamer. Values denote benzene molecule indices.

In principle, many different approximate FDE-diab(K, L, M) computational protocols can be constructed varying the parameters K , L , and M independently. However, here we will only consider those systematically converging to the full FDE-diab(8,8,8) solution. To that end, three major strategies can be applied: i) varying the number of states K keeping other parameters fixed, ii) changing the number of subsystems L contained in \mathcal{L} keeping other parameters fixed, and iii) simultaneously varying all three parameters. Note here that the number of subsystems M used for the construction of quasi-diabatic states defines the maximum values of K and L and, therefore, cannot be changed independently.

Because central benzene molecules 4 and 5 carry the largest spin-density contributions, it is reasonable to start from them and step-by-step vary the values of K , L , and M including contributions from the pairs of benzene molecules which are further away from the center. Keeping this in mind and constructing approximate protocols according to the three strategies described above, we introduce three series of approximations: FDE-diab($i,8,8$), $i = 2, 4, 6$, FDE-diab($8,i,8$), $i = 2, 4, 6$, and FDE-diab(i,i,i), $i = 2, 4, 6$. Using these three series of protocols, we calculate spin-density distributions of the benzene octamer and compare them against those computed with FDE-diab($8,8,8$). The difference spin-density distributions are shown in Fig. 5, whereas the values of molecular spin populations are given in Tab. S16 in the SI.

As can be seen from Fig. 5 and Tab. S16 in the SI, for $i = 2$ all computational protocols predict about 50% of the spin density being localized at each of benzene molecules 4 and 5. Neighboring molecules 3 and 6 carry only negligibly small amounts of the spin density (below 1%) for FDE-diab($2,8,8$) and FDE-diab($8,2,8$), while no spin polarization at benzene molecules 3 and 6 is present for FDE-diab($2,2,2$). The latter result is not surprising and is caused by the fact that only MOs of subsystems 4 and 5 were considered within FDE-diab($2,2,2$). Already the use of FDE-diab($4,8,8$) and FDE-diab($8,4,8$) produces spin-density distributions very similar to those from the FDE-diab($8,8,8$) computation. The corresponding approximate molecular spin populations deviate from the reference ones by less than 1%. Contrary to that, FDE-diab($4,4,4$) shows a slower convergence and leads to molecular spin populations deviating from FDE-diab($8,8,8$) by up to about 7%. However, this computational scheme produces much smaller deviations (below 2%) in the next step ($i = 6$), while the use of other two protocols leads to a slight increase in the error. Overall, all three approaches perform very similar and converge to the full FDE-diab solution with increasing i . From the practical point of view, however, FDE-diab($i,8,8$) is of little interest as it leads to the smallest reduction in the computational cost compared to the other two schemes.

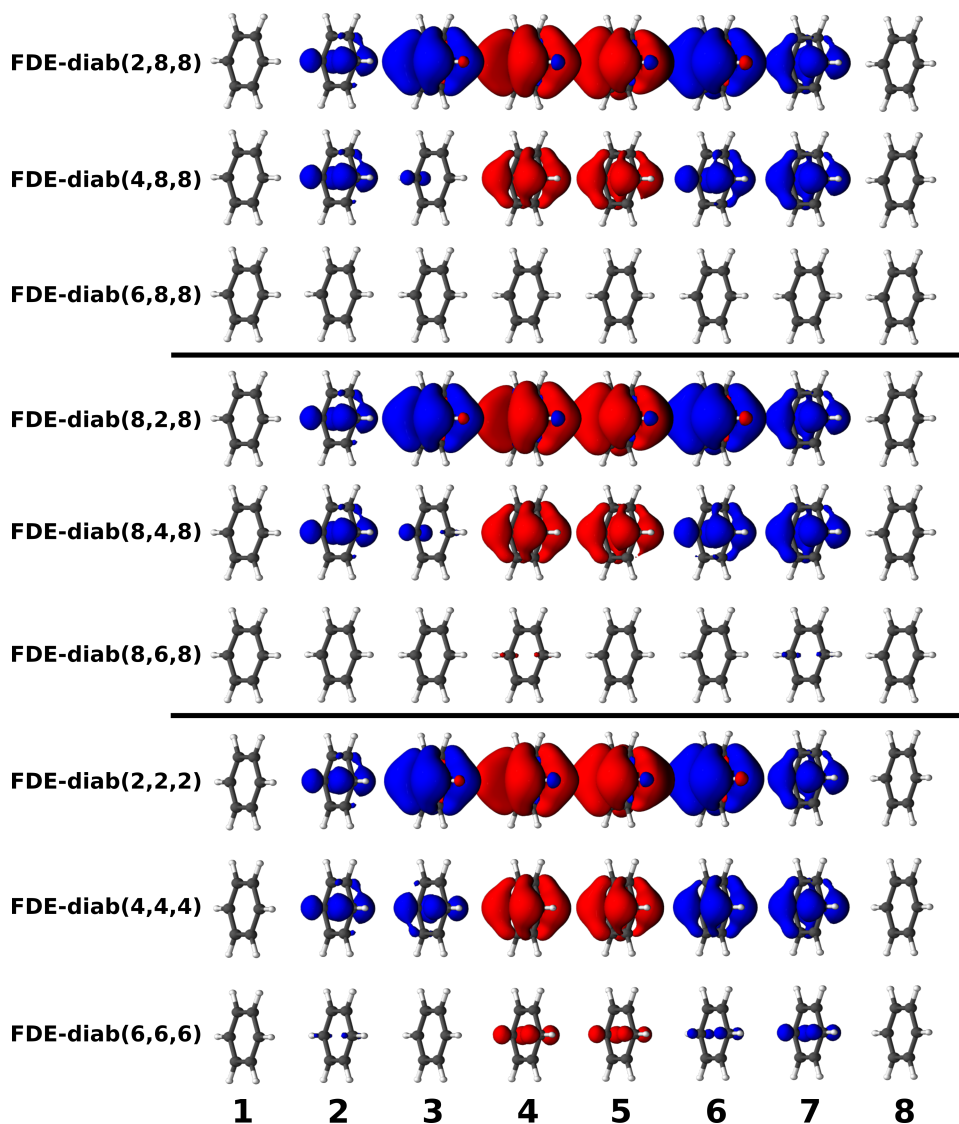


Figure 5: Difference ground state spin-density distributions (isovalue: ± 0.0003 a.u.; FDE-diab(8,8,8) spin density serves as the reference) calculated for the benzene octamer radical cation using approximate FDE-diab schemes. Results are shown for the three series of approximations converging to the full FDE-diab(8,8,8) limit: (top) FDE-diab(i , 8, 8) with $i = 2, 4, 6$, (middle) FDE-diab(8, i , 8) with $i = 2, 4, 6$, and (bottom) FDE-diab(i, i, i) with $i = 2, 4, 6$. Blue and red colors indicate positive and negative difference spin-density polarization, respectively. Benzene molecule indices are given with integer numbers.

5 Conclusions

In this work, we presented a multi-state extension of the recently reported FDE-diab [45, 49, 50] approach. This methodology is based on the FDE formalism and employs non-orthogonal quasi-diabatic states as a basis for qualitatively correct calculations of spin densities, electronic couplings, and excitation energies. We described the new FDE-diab implementation in the SERENITY program code and thoroughly tested the method. To that end, we first compared the performance of two-state FDE-diab implemented in the SERENITY and ADF program packages by calculating molecular properties such as electronic couplings, spin densities, and atomic spin populations. We showed that both implementations produce very similar results with only minor deviations caused by different basis set types used (GTO in SERENITY vs. STO in ADF).

Second, we validated the multi-state FDE-diab framework by calculating ground and excited state molecular properties of the DNA base triplets $[G_1AG_2]^{\bullet+}$ and $[G_1TG_2]^{\bullet+}$ and compared the obtained results against those from KS-DFT and the CASSCF reference. As expected, KS-DFT ground state spin-density distributions were strongly dependent on the XC functional used. Calculations employing double-hybrid B2PLYP led to the best agreement with CASSCF, but also featured large spin contamination values (spin expectation values $\langle S^2 \rangle$ of about 1.1 a.u.) and, as the result, overestimated areas of the negative spin density. Contrary to that, an impressive agreement with the CASSCF reference was found while using FDE-diab with the rather simple GGA-type XC functional PW91. In this case, qualitatively correct (compared to CASSCF) spin densities, molecular spin populations, and excitation energies were obtained for the three lowest electronic states of $[G_1AG_2]^{\bullet+}$ and $[G_1TG_2]^{\bullet+}$. The corresponding FDE-diab spin expectation values $\langle S^2 \rangle$ were equal to about 0.8 a.u. and, therefore, showed only a slight degree of spin contamination. Moreover, an excellent quantitative agreement with CASSCF was obtained for $[G_1TG_2]^{\bullet+}$ molecular spin populations (errors below 1.5%) and $[G_1AG_2]^{\bullet+}$ excitation

energies (deviations below 0.01 eV). It should be noted, however, that a rather small active space and no perturbation energy correction were employed in the reference CASSCF calculations. Therefore, somewhat larger deviations found for other molecular properties and complexes do not necessarily mean a worse performance of the FDE-diab approach.

Finally, we showed that the new multi-state FDE-diab framework implemented in the SERENITY program allows us to apply different combinations of approximate techniques reported previously for two-state FDE-diab and FDE-ET (see Refs. [46] and [49,50]). A unified notation system for these combinations was proposed. Using an example of a π -stacked benzene octamer radical, we demonstrated how these techniques can be applied to construct series of approximate approaches, which considerably reduce the overall computational cost and systematically converge to the full multi-state FDE-diab solution.

Summarizing the presented results, we conclude that the new multi-state FDE-diab approach is an effective tool for calculations of molecular properties such as spin densities, electronic couplings, and excitation energies. Our test computations demonstrate a surprisingly good agreement with the reference results and hint at the potential of FDE-diab to be a less expensive but accurate enough alternative to computationally very demanding CASSCF. The approximate techniques implemented within the multi-state FDE-diab framework allow one to target large molecular systems of biochemical interest. This is due to the favourable scaling behaviour of FDE-diab (and the underlying FDE method) with the number of subsystems [66]. Two-state FDE-diab calculations of photosynthetic reaction center models including large parts of the protein environments can serve as examples for large-scale calculations with this technique [49,50]. However, the developed methodology is based on FDE and, therefore, shares the same set of limitations including the inability to describe covalently bonded or strongly interacting fragments. This limitation is lifted by methods such as potential reconstruction [92–94], projection-based embedding [95–97] and three-partition FDE [98–100]. Whether these techniques can effectively be combined

with the FDE-diab methodology is an open question, which will be addressed elsewhere.

Acknowledgments

P.E. thanks Niklas Niemeyer for discussions on the SERENITY framework and Dr. Milica Feldt for her help with CASSCF calculations. D.G.A. acknowledges funding from the European Union's Horizon 2020 research and innovation programme under the Marie Skłodowska–Curie grant agreement no. 835776.

References

- [1] C. R. Jacob, M. Reiher. Spin in density-functional theory. *Int. J. Quantum Chem.*, **112**(23) (2012) 3661–3684.
- [2] J. Wang, A. D. Becke, V. H. Smith. Evaluation of $\langle S^2 \rangle$ in restricted, unrestricted Hartree–Fock, and density functional based theories. *J. Chem. Phys.*, **102**(8) (1995) 3477–3480.
- [3] K. Yamaguchi, Y. Takahara, T. Fueno. Ab-Initio Molecular Orbital Studies of Structure and Reactivity of Transition Metal-OXO Compounds. *Advances in Quantum Chemistry*, p. 155–184. Springer Netherlands: Dordrecht, 1986.
- [4] T. Soda, Y. Kitagawa, T. Onishi, Y. Takano, Y. Shigeta, H. Nagao, Y. Yoshioka, K. Yamaguchi. Ab Initio Computations of Effective Exchange Integrals for H–H, H–He–H and Mn_2O_2 Complex: Comparison of Broken-Symmetry Approaches. *Chem. Phys. Lett.*, **319** (2000) 223–230.
- [5] M. Deumal, M. J. Bearpark, J. J. Novoa, A. Michael M. A. Robb. Magnetic Properties of Organic Molecular Crystals via an Algebraic Heisenberg Hamiltonian. Applications to WILVIW, TOLKEK, and KAXHAS Nitronyl Nitroxide Crystals. *J. Phys. Chem. A*, **106**(7) (2002) 1299–1315.
- [6] T. Dresselhaus, S. Eusterwiemann, D. R. Matuschek, C. G. Daniliuc, O. Janka, R. Pöttgen, A. Studer, J. Neugebauer. Black-box determination of temperature-dependent susceptibilities for crystalline organic radicals with complex magnetic topologies. *Phys. Chem. Chem. Phys.*, **18** (2016) 28262–28273.
- [7] P. J. Brown. Polarized neutron diffraction. *Sci. Prog.*, **73**(2) (1989) 213–230.

- [8] R. J. Papoular, B. Gillon. Maximum Entropy Reconstruction of Spin Density Maps in Crystals from Polarized Neutron Diffraction Data. *Europhys. Lett.*, **13**(5) (1990) 429–434.
- [9] A. Zheludev, V. Barone, M. Bonnet, B. Delley, A. Grand, E. Ressouche, P. Rey, R. Subra, J. Schweizer. Spin density in a nitronyl nitroxide free radical. Polarized neutron diffraction investigation and ab initio calculations. *J. Am. Chem. Soc.*, **116**(5) (1994) 2019–2027.
- [10] M. Kaupp, M. Bühl, V. G. Malkin, Eds. *Calculation of NMR and EPR parameters: Theory and Applications*. WILEY-VCH Verlag GmbH & Co. KG, Weinheim, 2004.
- [11] D. Dolphin, R. H. Felton, D. C. Borg, J. Fajer. Isoporphyrins. *J. Am. Chem. Soc.*, **92** (1970) 743–745.
- [12] J. Fajer, M. S. Davis. Electron spin resonance of porphyrin π cations and anions. In D. Dolphin, Ed., *The Porphyrins, Volume IV, Physical Chemistry, Part B*. Academic Press, New York, 1979.
- [13] F. Lendzian, M. Huber, R. A. Isaacson, B. Endeward, M. Plato, B. Bönigk, K. Möbius, W. Lubitz, G. Feher. The electronic structure of the primary donor cation radical in *Rhodobacter sphaeroides* R-26: ENDOR and TRIPLE resonance studies in single crystals of reaction centers. *Biochim. Biophys. Acta*, **1183** (1993) 139–160.
- [14] H. Käß, E. Bittersmann-Weidlich, L.-E. Andréasson, B. Bönigk, W. Lubitz. ENDOR and ESEEM of the ^{15}N labelled radical cations of chlorophyll a and the primary donor P700 in photosystem I. *Chem. Phys.*, **194** (1995) 419–432.
- [15] W. Lubitz. Pulse EPR and ENDOR studies of light-induced radicals and triplet states in photosystem II of oxygenic photosynthesis. *Phys. Chem. Chem. Phys.*, **4** (2002) 5539–5545.

- [16] E. Daviso, S. Prakash, A. Alia, P. Gast, J. Neugebauer, G. Jeschke, J. Matysik. The electronic structure of the primary electron donor of reaction centers of purple bacteria at atomic resolution as observed by photo-CIDNP ^{13}C NMR. *PNAS*, **106** (2009) 22281–22286.
- [17] G. J. Janssen, E. Daviso, M. van Son, H. J. M. de Groot, A. Alia, J. Matysik. Observation of the solid-state photo-CIDNP effect in entire cells of cyanobacteria *Synechocystis*. *Photosynth. Res.*, **104** (2010) 275–282.
- [18] M. Najdanova, G. J. Janssen, H. J. M. de Groot, J. Matysik, A. Alia. Analysis of electron donors in photosystems in oxygenic photosynthesis by photo-CIDNP MAS NMR. *J. Photochem. Photobiol. B*, **152** (2015) 261–271.
- [19] G. J. Janssen, P. Bielytskyi, D. G. Artiukhin, J. Neugebauer, H. J. M. de Groot, J. Matysik, A. Alia. Photochemically induced dynamic nuclear polarization NMR on photosystem II: donor cofactor observed in entire plant. *Sci. Rep.*, **8** (2018) 17853.
- [20] T. Bally, W. T. Borden. *Calculations on Open-Shell Molecules: A Beginner's Guide*, p. 1–97. John Wiley & Sons, Ltd, 1999.
- [21] M. Reiher. A Theoretical Challenge: Transition-Metal Compounds. *Chimia*, **63** (2009) 140–145.
- [22] K. Boguslawski, C. R. Jacob, M. Reiher. Can DFT Accurately Predict Spin Densities? Analysis of Discrepancies in Iron Nitrosyl Complexes. *J. Chem. Theory Comput.*, **7**(9) (2011) 2740–2752.
- [23] M. Radoń, E. Broclawik, K. Pierloot. Electronic Structure of Selected FeNO_7 Complexes in Heme and Non-Heme Architectures: A Density Functional and Multireference ab Initio Study. *J. Phys. Chem. B*, **114**(3) (2010) 1518–1528.

- [24] S. Kossmann, F. Neese. Correlated *ab Initio* Spin Densities for Larger Molecules: Orbital-Optimized Spin-Component-Scaled MP2 Method. *J. Phys. Chem. A*, **114**(43) (2010) 11768–11781.
- [25] K. Boguslawski, K. H. Marti, Ö. Legeza, M. Reiher. Accurate *ab Initio* Spin Densities. *J. Chem. Theory Comput.*, **8**(6) (2012) 1970–1982.
- [26] T. N. Lan, Y. Kurashige, T. Yanai. Toward Reliable Prediction of Hyperfine Coupling Constants Using *Ab Initio* Density Matrix Renormalization Group Method: Diatomic $^2\Sigma$ and Vinyl Radicals as Test Cases. *J. Chem. Theory Comput.*, **10**(5) (2014) 1953–1967.
- [27] T. Shiozaki, T. Yanai. Hyperfine Coupling Constants from Internally Contracted Multireference Perturbation Theory. *J. Chem. Theory Comput.*, **12**(9) (2016) 4347–4351.
- [28] P. Mori-Sánchez, A. J. Cohen, W. Yang. Many-electron self-interaction error in approximate density functionals. *J. Chem. Phys.*, **125** (2006) 201102.
- [29] J. Gräfenstein, E. Kraka, D. Cremer. Effect of the self-interaction error for three-electron bonds: On the development of new exchange-correlation functionals. *Phys. Chem. Chem. Phys.*, **6** (2004) 1096–1112.
- [30] A. J. Cohen, P. Mori-Sánchez, W. Yang. Development of exchange-correlation functionals with minimal many-electron self-interaction error. *J. Chem. Phys.*, **126** (2007) 191109.
- [31] A. J. Cohen, P. Mori-Sánchez, W. Yang. Insights into Current Limitations of Density Functional Theory. *Science*, **321** (2008) 792–794.
- [32] A. Solovyeva, M. Pavanello, J. Neugebauer. Spin densities from subsystem density-functional theory: Assessment and application to a photosynthetic reaction center complex model. *J. Chem. Phys.*, **136** (2012) 194104.

- [33] C. Herrmann, M. Reiher, B. A. Hess. Comparative analysis of local spin definitions. *J. Chem. Phys.*, **122** (2005) 034102.
- [34] C. Herrmann, L. Yu, M. Reiher. Spin States in Polynuclear Clusters: The [Fe₂O₂] Core of the Methane Monooxygenase Active Site. *J. Comput. Chem.*, **27** (2006) 1223–1239.
- [35] A. J. Cohen, D. J. Tozer, N. C. Handy. Evaluation of $\langle \hat{S}^2 \rangle$ in density functional theory. *J. Chem. Phys.*, **126** (2007) 214104.
- [36] A. S. Menon, L. Radom. Consequences of Spin Contamination in Unrestricted Calculations on Open-Shell Species: Effect of Hartree–Fock and Møller–Plesset Contributions in Hybrid and Double-Hybrid Density Functional Theory Approaches. *J. Phys. Chem. A*, **112** (2008) 13225–13230.
- [37] M. Pavanello, J. Neugebauer. Modelling charge transfer reactions with the frozen density embedding formalism. *J. Chem. Phys.*, **135** (2011) 234103.
- [38] A. Solovyeva, M. Pavanello, J. Neugebauer. Spin densities from subsystem density-functional theory: Assessment and application to a photosynthetic reaction center complex model. *J. Chem. Phys.*, **136**(19) (2012) 194104.
- [39] D. G. Artiukhin, C. J. Stein, M. Reiher, J. Neugebauer. Quantum Chemical Spin Densities for Radical Cations of Photosynthetic Pigment Models. *Photochem. Photobiol.*, **93** (2017) 815–833.
- [40] T. A. Wesolowski, A. Warshel. Frozen density functional approach for ab initio calculations of solvated molecules. *J. Phys. Chem.*, **97** (1993) 8050–8053.
- [41] T. A. Wesolowski, J. Weber. Kohn–Sham equations with constrained electron density: An iterative evaluation of the ground-state electron density of interacting molecules. *Chem. Phys. Lett.*, **248** (1996) 71–76.

- [42] T. A. Wesolowski. Density functional theory with approximate kinetic energy functionals applied to hydrogen bonds. *J. Chem. Phys.*, **106**(20) (1997) 8516–8526.
- [43] T. A. Wesolowski. *Computational Chemistry: Reviews of Current Trends*, Volume 10, Chapter One-Electron Equations for Embedded Electron Density: Challenge for Theory and Practical Payoffs in Multi-Level Modelling of Complex Polyatomic Systems, p. 1–82. World Scientific, 2006.
- [44] D. Schnieders, J. Neugebauer. Accurate embedding through potential reconstruction: A comparison of different strategies. *J. Chem. Phys.*, **149**(5) (2018) 054103.
- [45] D. G. Artiukhin, J. Neugebauer. Frozen-density embedding as a quasi-diabatization tool: Charge-localized states for spin-density calculations. *J. Chem. Phys.*, **148** (2018) 214104.
- [46] M. Pavanello, T. Van Voorhis, L. Visscher, J. Neugebauer. An accurate and linear-scaling method for calculating charge-transfer excitation energies and diabatic couplings. *J. Chem. Phys.*, **138** (2013) 054101.
- [47] A. Solovyeva, M. Pavanello, J. Neugebauer. Describing long-range charge-separation processes with subsystem density-functional theory. *J. Chem. Phys.*, **140** (2014) 164103.
- [48] P. Ramos, M. Papadakis, M. Pavanello. Performance of Frozen Density Embedding for Modeling Hole Transfer Reactions. *J. Phys. Chem. B*, **119** (2015) 7541–7557.
- [49] D. G. Artiukhin, P. Eschenbach, J. Neugebauer. Computational Investigation of the Spin-Density Asymmetry in Photosynthetic Reaction Center Models from First Principles. *J. Phys. Chem. B*, **124**(24) (2020) 4873–4888.
- [50] D. G. Artiukhin, P. Eschenbach, J. Matysik, J. Neugebauer. Theoretical Assessment of Hinge-Type Models for Electron Donors in Reaction Centers of Photosystems I and II as Well as of Purple Bacteria. *J. Phys. Chem. B*, **125**(12) (2021) 3066–3079.

- [51] A. Migliore, S. Corni, D. Versano, M. L. Klein, R. Di Felice. First Principles Effective Electronic Couplings for Hole Transfer in Natural and Size-Expanded DNA. *J. Phys. Chem. B*, **113** (2009) 9402–9415.
- [52] A. Migliore. Nonorthogonality Problem and Effective Electronic Coupling Calculation: Application to Charge Transfer in π -Stacks Relevant to Biochemistry and Molecular Electronics. *J. Chem. Theory Comput.*, **7** (2011) 1712–1725.
- [53] T. A. Wesolowski. Application of the DFT-based embedding scheme using an explicit functional of the kinetic energy to determine the spin density of Mg^+ embedded in Ne and Ar matrices. *Chem. Phys. Lett.*, **311**(1) (1999) 87–92.
- [54] P.-O. Löwdin. Quantum theory of many-particle systems. I. Physical interpretations by means of density matrices, natural spin-orbitals, and convergence problems in the method of configurational interaction. *Phys. Rev.*, **97** (1955) 1474–1489.
- [55] I. Mayer. *Simple Theorems, Proofs, and Derivations in Quantum Chemistry*. Kluwer Academic/Plenum, 2003.
- [56] L. Blancafort, A. A. Voityuk. CASSCF/CAS-PT2 Study of Hole Transfer in Stacked DNA Nucleobases. *J. Phys. Chem. A*, **110**(20) (2006) 6426–6432.
- [57] A. Kubas, F. Hoffmann, A. Heck, H. Oberhofer, M. Elstner, J. Blumberger. Electronic couplings for molecular charge transfer: Benchmarking CDFT, FODFT, and FODFTB against high-level ab initio calculations. *J. Chem. Phys.*, **140**(10) (2014) 104105.
- [58] M. D. Hanwell, D. E. Curtis, D. C. Lonie, T. Vandermeersch, E. Zurek, G. R. Hutchison. Avogadro: an advanced semantic chemical editor, visualization, and analysis platform. *J. Cheminformatics*, **4** (2012) 17.

- [59] R. Ahlrichs, M. Bär, M. Häser, H. Horn, C. Kölmel. Electronic structure calculations on workstation computers: The program system turbomole. *Chem. Phys. Lett.*, **162** (1989) 165–169.
- [60] A. Schäfer, H. Horn, R. Ahlrichs. Fully optimized contracted Gaussian basis sets for atoms Li to Kr. *J. Chem. Phys.*, **97** (1992) 2571–2577.
- [61] A. Schäfer, C. Huber, R. Ahlrichs. Fully optimized contracted Gaussian basis sets of triple zeta valence quality for atoms Li to Kr. *J. Chem. Phys.*, **100** (1994) 5829.
- [62] J. P. Perdew, M. Ernzerhof, K. Burke. Rationale for mixing exact exchange with density functional approximations. *J. Chem. Phys.*, **105** (1996) 9982–9985.
- [63] C. Adamo, V. Barone. Toward reliable density functional methods without adjustable parameters: The PBE0 model. *J. Chem. Phys.*, **100** (1999) 6158–6170.
- [64] S. Grimme, J. Antony, S. Ehrlich, H. Krieg. A consistent and accurate ab initio parametrization of density functional dispersion correction (DFT-D) for the 94 elements H-Pu. *J. Chem. Phys.*, **132** (2010) 154104.
- [65] S. Grimme, S. Ehrlich, L. Goerigk. Effect of the damping function in dispersion corrected density functional theory. *J. Comput. Chem.*, **32** (2011) 1456–1465.
- [66] J. P. Unsleber, T. Dresselhaus, K. Klahr, D. Schnieders, M. Böckers, D. Barton, J. Neugebauer. SERENITY: A subsystem quantum chemistry program. *J. Comput. Chem.*, **39** (2018) 788–798.
- [67] Amsterdam density functional program, Theoretical Chemistry, Vrije Universiteit, Amsterdam, URL: <http://www.scm.com>, access date: 25 August 2021.
- [68] C. R. Jacob, J. Neugebauer, L. Visscher. A flexible implementation of frozen-density embedding for use in multilevel simulations. *J. Comput. Chem.*, **29**(6) (2008) 1011–1018.

- [69] E. van Lenthe, E. J. Baerends. Optimized Slater-type basis sets for the elements 1-118. *J. Comput. Chem.*, **24** (2003) 1142–1156.
- [70] J. P. Perdew, K. Burke, M. Ernzerhof. Generalized Gradient Approximation Made Simple. *Phys. Rev. Lett.*, **77** (1996) 3865–3868.
- [71] A. D. Becke. Density-functional thermochemistry. III. The role of exact exchange. *J. Chem. Phys.*, **98**(7) (1993) 5648–5652.
- [72] C. Lee, W. Yang, R. G. Parr. Development of the Colle-Salvetti correlation-energy formula into a functional of the electron density. *Phys. Rev. B*, **37** (1988) 785–789.
- [73] S. H. Vosko, L. Wilk, M. Nusair. Accurate spin-dependent electron liquid correlation energies for local spin density calculations: a critical analysis. *Can. J. Phys.*, **58**(8) (1980) 1200–1211.
- [74] P. J. Stephens, F. J. Devlin, C. F. Chabalowski, M. J. Frisch. Ab Initio Calculation of Vibrational Absorption and Circular Dichroism Spectra Using Density Functional Force Fields. *J. Phys. Chem.*, **98**(45) (1994) 11623–11627.
- [75] M. Seth, T. Ziegler. Range-Separated Exchange Functionals with Slater-Type Functions. *J. Chem. Theory Comput.*, **8**(3) (2012) 901–907.
- [76] S. Grimme. Semiempirical hybrid density functional with perturbative second-order correlation. *J. Chem. Phys.*, **124**(3) (2006) 034108.
- [77] J. P. Perdew, J. A. Chevary, S. H. Vosko, K. A. Jackson, M. R. Pederson, D. J. Singh, C. Fiolhais. Atoms, molecules, solids, and surfaces: Applications of the generalized gradient approximation for exchange and correlation. *Phys. Rev. B*, **46** (1992) 6671.
- [78] J. P. Perdew, Y. Wang. *Electronic Structure of Solids91*. Akademie, Berlin, 1991.
- [79] H. Lee, C. Lee, R. G. Parr. Conjoint gradient correction to the Hartree–Fock kinetic- and exchange-energy density functionals. *Phys. Rev. A*, **44** (1991) 768–771.

- [80] A. Lembarki, H. Chermette. Obtaining a gradient-corrected kinetic-energy functional from the Perdew–Wang exchange functional. *Phys. Rev. A*, **50** (1994) 5328–5331.
- [81] A. D. Becke. A multicenter numerical integration scheme for polyatomic molecules. *J. Chem. Phys.*, **88**(4) (1988) 2547–2553.
- [82] O. Treutler, R. Ahlrichs. Efficient molecular numerical integration schemes. *J. Chem. Phys.*, **102** (1995) 346.
- [83] M. Franchini, P. H. T. Philipsen, L. Visscher. The Becke Fuzzy Cells Integration Scheme in the Amsterdam Density Functional Program Suite. *J. Comput. Chem.*, **34** (2013) 1819.
- [84] B. O. Roos, P. R. Taylor, P. E. M. Sigbahn. A complete active space SCF method (CASSCF) using a density matrix formulated super-CI approach. *Chem. Phys.*, **48**(2) (1980) 157–173.
- [85] K. Ruedenberg, M. W. Schmidt, M. M. Gilbert, S. T. Elbert. Are atoms intrinsic to molecular electronic wavefunctions? I. The FORS model. *Chem. Phys.*, **71**(1) (1982) 41–49.
- [86] J. Olsen. The CASSCF method: A perspective and commentary. *Int. J. Quantum Chem.*, **111**(13) (2011) 3267–3272.
- [87] I. F. Galván, M. Vacher, A. Alavi, C. Angeli, F. Aquilante, J. Autschbach *et al.* OpenMolcas: From Source Code to Insight. *J. Chem. Theory Comp.*, **15**(11) (2019) 5925–5964.
- [88] F. Aquilante, J. Autschbach, A. Baiardi, S. Battaglia, V. A. Borin, L. F. Chibotaru *et al.* Modern quantum chemistry with [Open]Molcas. *J. Chem. Phys.*, **152**(21) (2020) 214117.

- [89] T. H. Dunning. Gaussian basis sets for use in correlated molecular calculations. I. The atoms boron through neon and hydrogen. *J. Chem. Phys.*, **90**(2) (1989) 1007–1023.
- [90] D. E. Woon, T. H. Dunning. Gaussian basis sets for use in correlated molecular calculations. III. The atoms aluminum through argon. *J. Chem. Phys.*, **98**(2) (1993) 1358–1371.
- [91] L. Blancafort, A. A. Voityuk. MS-CASPT2 Calculation of Excess Electron Transfer in Stacked DNA Nucleobases. *J. Phys. Chem. A*, **111**(21) (2007) 4714–4719.
- [92] R. van Leeuwen, E. J. Baerends. Exchange-correlation potential with correct asymptotic behavior. *Phys. Rev. A*, **49** (1994) 2421–2431.
- [93] Q. Wu, W. Yang. A direct optimization method for calculating density functionals and exchange–correlation potentials from electron densities. *J. Chem. Phys.*, **118**(6) (2003) 2498–2509.
- [94] X. Zhang, E. A. Carter. Kohn-Sham potentials from electron densities using a matrix representation within finite atomic orbital basis sets. *J. Chem. Phys.*, **148**(3) (2018) 034105.
- [95] S. Huzinaga, A. A. Cantu. Theory of Separability of Many-Electron Systems. *J. Chem. Phys.*, **55**(12) (1971) 5543–5549.
- [96] F. R. Manby, M. Stella, J. D. Goodpaster, T. F. Miller. A Simple, Exact Density-Functional-Theory Embedding Scheme. *J. Chem. Theory Comput.*, **8**(8) (2012) 2564–2568.
- [97] Y. G. Khait, M. R. Hoffmann. Chapter Three — On the Orthogonality of Orbitals in Subsystem Kohn–Sham Density Functional Theory. In R. A. Wheeler, Ed., *Annual Reports in Computational Chemistry*, Volume 8, p. 53–70. Elsevier, 2012.

- [98] C. R. Jacob, L. Visscher. A subsystem density-functional theory approach for the quantum chemical treatment of proteins. *J. Chem. Phys.*, **128**(15) (2008) 155102.
- [99] S. Fux, C. R. Jacob, J. Neugebauer, L. Visscher, M. Reiher. Accurate frozen-density embedding potentials as a first step towards a subsystem description of covalent bonds. *J. Chem. Phys.*, **132**(16) (2010) 164101.
- [100] K. Kiewisch, C. R. Jacob, L. Visscher. Quantum-Chemical Electron Densities of Proteins and of Selected Protein Sites from Subsystem Density Functional Theory. *J. Chem. Theory Comput.*, **9**(5) (2013) 2425–2440.